SAR TOMOGRAPHY BASED 3-D POINT CLOUD EXTRACTION OF POINT-LIKE SCATTERERS IN URBAN AREAS

Othmar Frey
Earth Observation & Remote Sensing
ETH Zurich, Switzerland /
Gamma Remote Sensing
Switzerland
Email: otfrey@ethz.ch

Irena Hajnsek
Earth Observation & Remote Sensing
ETH Zurich, Switzerland /
German Aerospace Center - DLR,
Germany

Urs Wegmuller, Charles L. Werner
Gamma Remote Sensing
Switzerland

***Abstract*—SAR tomography as an extension to persistent scatterer interferometry (PSI) approaches has the potential to improve the level of detail of retrievable information, in particular, in the case of layover scenarios in urban areas. In this paper, a processing approach is sketched that eventually allows for retrieving a 3-D point cloud of point-like scatterers based on subsequent PSI and SAR tomography processing of an interferometric stack of high-resolution spaceborne TerraSAR-X data acquired over the city of Barcelona between the years 2008 and 2012. Experimental results are presented in the form of (1) vertical tomographic slices of high-rise buildings and (2) a 3-D point cloud of a larger district of the city of Barcelona retrieved from the tomograms.**

***Index Terms*—Synthetic aperture radar (SAR), SAR tomography, SAR interferometry, persistent scatterer interferometry, interferometric stacking, spaceborne SAR, 3-D point cloud**

I. Introduction

The high-resolution nature of spaceborne synthetic aperture radar (SAR) sensors, such as TerraSAR-X, leads to a much higher number of detectable point-like scatterers that are coherent over time. The concept of SAR tomography provides a means to overcome the restriction of conventional persistent scatterer interferometry, namely, that only one scatterer is present in a particular resolution cell. Taking advantage of the elevation dimension by means of SAR tomography adds valuable information about the structure of complex target scenarios, such as urban areas (or forests). Three-dimensional imaging of such scenarios from multibaseline SAR data has been discussed by a number of authors [1]–[5] and [6]–[13]. In the spaceborne case, ideally 25 up to 50 or even 100 repeat-pass interferometric data sets of the same area with spatial baselines perpendicular to the line of sight are required to resolve targets also in the elevation direction.

In this paper, we present the status and our most recent results of our efforts to combine SAR tomography with an operational interferometric point target analysis (IPTA) software as an extension to conventional PSI processing.

Experimental results based on an interferometric stack of TerraSAR-X data over the city of Barcelona are presented. In particular, we show (1) tomographic slices of high-rise buildings obtained by means of computationally efficient approaches such as Tikhonov-regularized inversion and (2) a three-dimensional point cloud of a larger district of the city of Barcelona obtained through tomographic processing and local peak detection.

II. Methods

SAR tomography processing of spaceborne repeat-pass SAR data requires that, prior to be able to perform tomographic focusing in the elevation direction, a PSI processing sequence is performed to extract and remove the atmospheric phase contributions [14]. Preprocessing steps include the selection of a reference scene from a stack of SLC images, geocoding the data using the multilook intensity image of the reference scene [15], [16], and coregistration including a refinement step using offset estimates between the data sets of the stack. After a preselection of point target candidates, based on spectral diversity and the temporal variability of the backscattering, point differential interferograms are obtained interactively. The topographic and orbital phases are then simulated and subtracted from the point-wise complex-valued interferogram followed by unwrapping and filtering to isolate the spatially correlated phase contributions from high-frequency phase contributions such as the residual topographic phase. When a PSI solution is obtained, the low-frequency

phase contributions are expanded to the full SLCs again, such that tomographic focusing can potentially be performed at each pixel location in the SLC to find additional multiple scatterers in one range-azimuth resolution cell.

The underlying assumption for the system model is of quasi-deterministic nature. Very few, typically one or two, dominant point-like scatterers are expected to be found in a resolution cell, and these scatterers are assumed to have a relatively stable target phase over the entire time series. The system model can be written as follows:

The complex reflectivity s of a point target source is

$$s = \alpha e^{i\phi}, \tag{1}$$

where α is the amplitude and ϕ is the phase of s. The complex demodulated signal vector $\mathbf{y}$ for source s is

$$\mathbf{y} = \mathbf{a}s \tag{2}$$

where $\mathbf{a} = [1\ e^{i\varphi_2} \dots e^{i\varphi_K}]^T$ is the steering vector with $\varphi_m = -2k_c(r_m - r_1)$, $m = 1 \dots K$; k_c is the central wavenumber and r_m is the range distance from the point scatterer to the m-th sensor position. For p point target sources the signal vector $\mathbf{y}$, which represents the signal impinging on the antenna array synthesized by the different orbit locations of the various SLC acquisition in elevation direction, yields

$$\mathbf{y} = \begin{bmatrix} \mathbf{a}_1 & \dots & \mathbf{a}_p \end{bmatrix} \begin{bmatrix} s_1 \\ \vdots \\ s_p \end{bmatrix} = \mathbf{B}\mathbf{s}. \tag{3}$$

The matrix $[\mathbf{a}_1 \dots \mathbf{a}_p]$ is summarized in matrix $\mathbf{B}$ called the steering matrix.

The beamforming-based tomographic reconstruction of the complex reflectivity $\hat{\mathbf{s}}$ along the elevation direction is obtained by

$$\hat{\mathbf{s}} = \mathbf{B}^H \mathbf{y}. \tag{4}$$

As a consequence of the non-uniform sampling of the tomography data the reconstructed profile in the elevation direction is usually affected by spurious side lobes. A tomographic inversion method that regularizes the sampling geometry is the truncated singular value decomposition (TSVD) approach as it has been suggested and applied in the context of SAR tomography in [17]. It starts with a singular value decomposition of the steering matrix $\mathbf{B} = \mathbf{U}\mathbf{\Sigma}\mathbf{V}^H$. Depending on the decay pattern of the singular values σ_n stored in the diagonal matrix Σ, a noise threshold is set at the Q-th singular value. All singular values $\sigma_n, n = Q+1, ..., K$ that lie below this threshold, as well as their corresponding orthogonal vectors $\mathbf{u}_n$, $\mathbf{v}_n$, are discarded. The inversion is then performed via the truncated pseudo-inverse $\mathbf{V}_{1,Q}(\mathbf{\Sigma}^{-1})_{1,Q}\mathbf{U}_{1,Q}^H$ of the steering matrix $\mathbf{B}$:

$$\hat{\mathbf{s}} = \mathbf{V}_{1,Q}(\mathbf{\Sigma}^{-1})_{1,Q}\mathbf{U}_{1,Q}^H\mathbf{y} \tag{5}$$

$\mathbf{B}$ is the steering matrix of size $K \times N_r$, where K is the number of acquisitions and N_r is the number of equally-spaced locations at which the profile in elevation direction is inverted. Instead of setting a hard threshold at a specific singular value a Tikhonov-regularized inversion can be performed. In this case, the inverse singular values $\sigma_{n_{rt}}^{-1}$ of the matrix $\mathbf{\Sigma}^{-1}$ in eq. (5) are replaced by the following weighting function:

$$\sigma_{n_{rt}}^{-1} = \frac{\sigma_n}{\sigma_n^2 + \epsilon^2}, \quad \epsilon = \sqrt{\frac{K}{K-Q}\sum_{n=Q+1}^{K} |\mathbf{U}_{Q+1,K}^H\mathbf{y}|^2}. \tag{6}$$

ϵ^2 is the noise power level which is estimated from the projection of the measured data to the noise space [5].

III. Implementation Aspects

The tomographic processing algorithms were implemented as computationally efficient ANSI C programs making use of the Linear Algebra Package (LAPACK) and Basic Linear Algebra Subprograms (BLAS) libraries. Efficiency during tomographic processing will become even more important once it will be used as a more operational extension to conventional PSI processing.

IV. Data

The data set used for the experiment consists of an interferometric stack of 45 TerraSAR-X stripmap-mode SLCs. The data was acquired over the city of Barcelona between 2008 and 2012.

V. Results

Figs. 1 & 2 show details of the resolved layover-situation for two high-rise buildings, Torre Agbar and Torre MAPFRE close to the Olympic Village in Barcelona. For both close-ups the temporally averaged multi-look intensity image and the corresponding tomographic transect in range/elevation as well as the extracted raw point cloud are shown.

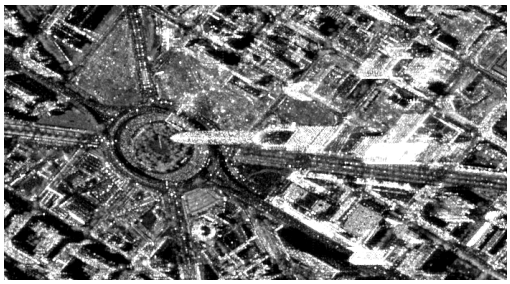

(a)

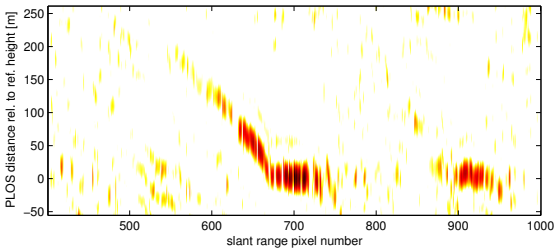

(b)

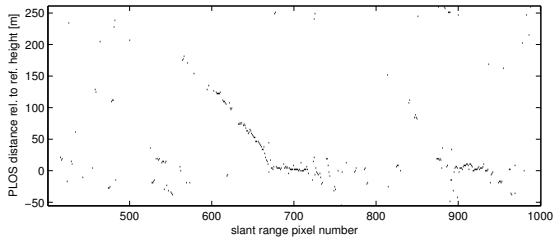

(c)

Fig. 1. (a) Subset of the averaged intensity image of the TerraSAR-X interferometric stack showing the layover situation for the Torre Agbar and surrounding buildings in Barcelona. (b) Tomographic slice showing the slant range / elevation plane of extended layover situation off the high-rise building Torre Agbar. Focusing algorithm: single-look Tikhonov-regularized inversion. (c) Extracted locations of stable scatterer candidates using a 2-peak detector.

(a)

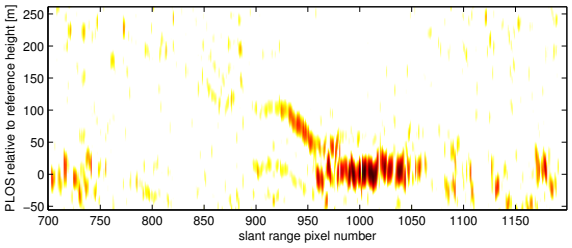

(b)

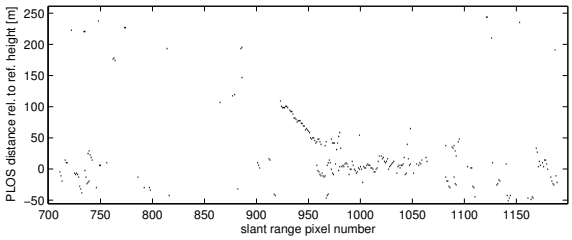

(c)

Fig. 2. (a) Subset of the averaged intensity image of the TerraSAR-X interferometric stack showing the layover situation for a tower close to the Olimpic Village in Barcelona. (b) Tomographic slice showing the slant range / elevation plane of extended layover situation off a high-rise building close to the Olimpic Village. Focusing algorithm: single-look Tikhonov-regularized inversion. (c) Extracted locations of stable scatterer candidates using a 2-peak detector.

In Fig. 3, the three-dimensional point cloud obtained by subsequent PSI and tomographic processing followed by a 2-peak detector with additional power thresholds is shown. The colour coding represents the relative height of each individual point with respect to the reference DSM (SRTM).

VI. Discussion

The tomographic slices in the vertical plane show a good side-lobe suppression. The tomographic profiles of the high-rise buildings (Figs. 1 & 2) demonstrate how the layover situation can be resolved. Up to two scatterers per resolution cell are identified and extracted using a local peak detector. Towards the upper end of the two towers the backscattering signal is defocused or weaker—a potential source is cyclic motion, which is not taken into account in the current inversion process. Due to the high point density, a lot of details of the urban structure can be perceived when examining the 3-D point cloud shown in Fig. 3. Visible features include elements of building blocks and infrastructure elements found along large streets and avenues. SAR tomography algorithms of the type of the Tikhonov-regularized inversion are computationally efficient; a drawback is a limited resolution compared to, e.g. compressive sensing approaches, which in contrast are computationally extremely expensive.

Acknowledgment

This research project is funded by the Swiss Space Office, State Secretariat for Education and Research of the Swiss Confederation (SER/SSO), through the MdP2012 initiative. TerraSAR-X SAR data over Barcelona was obtained courtesy of the German Aerospace Center DLR through proposal MTH1717. SRTM ©USGS.

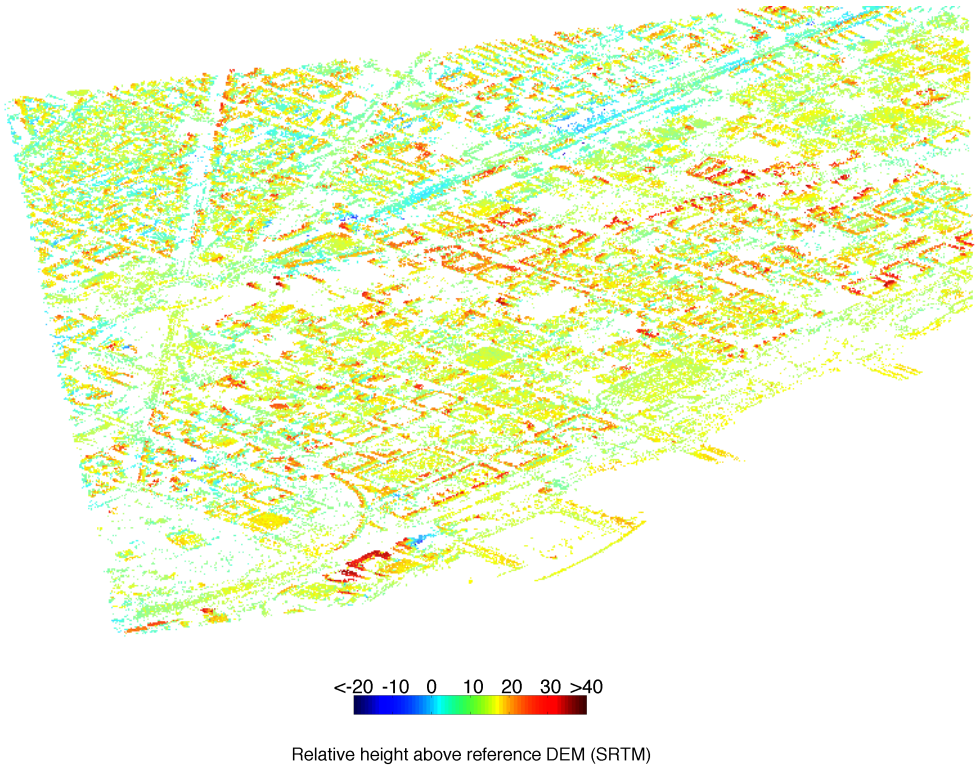

Fig. 3. 3-D point cloud of point-like scatterers obtained by Tikhonov-regularized tomographic processing of an interferometric stack of 45 stripmap-mode TerraSAR-X SLCs over the city of Barcelona. The colour coding represents the relative height with respect to the SRTM height model used as a reference.

REFERENCES

[1] G. Fornaro and A. Pauciullo, "LMMSE 3-D SAR focusing," *IEEE Trans. Geosci. Remote Sens.*, vol. 47, no. 1, pp. 214–223, Jan. 2009.

[2] G. Fornaro and F. Serafino, "Imaging of single and double scatterers in urban areas via SAR tomography," *IEEE Trans. Geosci. Remote Sens.*, vol. 44, no. 12, pp. 3497–3505, 2006.

[3] S. Sauer, L. Ferro-Famil, A. Reigber, and E. Pottier, "Three-dimensional imaging and scattering mechanism estimation over urban scenes using dual-baseline polarimetric InSAR observations at L-band," *IEEE Trans. Geosci. Remote Sens.*, vol. PP, no. 99, pp. 1–14, 2011.

[4] D. Reale, G. Fornaro, A. Pauciullo, X. X. Zhu, and R. Bamler, "Tomographic imaging and monitoring of buildings with very high resolution SAR data," *IEEE Geosci. Remote Sens. Lett.*, vol. 8, no. 4, pp. 661–665, July 2011.

[5] X. X. Zhu and R. Bamler, "Very high resolution spaceborne SAR tomography in urban environment," *IEEE Trans. Geosci. Remote Sens.*, vol. 48, no. 12, pp. 4296–4308, Dec. 2010.

[6] A. Reigber and A. Moreira, "First Demonstration of Airborne SAR Tomography Using Multibaseline L-Band Data," *IEEE Transactions on Geoscience and Remote Sensing*, vol. 38, no. 5, pp. 2142–2152, 2000.

[7] O. Frey and E. Meier, "Analyzing tomographic SAR data of a forest with respect to frequency, polarization, and focusing technique," *IEEE Trans. Geosci. Remote Sens.*, vol. 49, no. 10, pp. 3648–3659, Oct. 2011.

[8] O. Frey and E. Meier, "3-D time-domain SAR imaging of a forest using airborne multibaseline data at L- and P-bands," *IEEE Trans. Geosci. Remote Sens.*, vol. 49, no. 10, pp. 3660–3664, Oct. 2011.

[9] O. Frey, F. Morsdorf, and E. Meier, "Tomographic Imaging of a Forested Area By Airborne Multi-Baseline P-Band SAR," *Sensors, Special Issue on Synthetic Aperture Radar*, vol. 8, no. 9, pp. 5884–5896, sep 2008.

[10] O. Frey, I. Hajnsek, and U. Wegmuller, "Spaceborne SAR tomography in urban areas," in *Proc. IEEE Int. Geosci. Remote Sens. Symp.*, 2013, pp. 69–72.

[11] E. Aguilera, M. Nannini, and A. Reigber, "Multisignal compressed sensing for polarimetric SAR tomography," *IEEE Geosci. Remote Sens. Lett.*, vol. 5, no. 9, pp. 871–875, Sept. 2012.

[12] S. Tebaldini, "Single and multipolarimetric SAR tomography of forested areas: A parametric approach," *IEEE Trans. Geosci. Remote Sens.*, vol. 48, no. 5, pp. 2375–2387, May 2010.

[13] M. Nannini, R. Scheiber, R. Horn, and A. Moreira, "First 3-d reconstructions of targets hidden beneath foliage by means of polarimetric sar tomography," *IEEE Geoscience and Remote Sensing Letters*, vol. 9, no. 1, pp. 60 –64, jan. 2012.

[14] U. Wegmuller, D. Walter, V. Spreckels, and C. Werner, "Nonuniform ground motion monitoring with terrasar-x persistent scatterer interferometry," *Geoscience and Remote Sensing, IEEE Transactions on*, vol. 48, no. 2, pp. 895 –904, feb. 2010.

[15] U. Wegmuller, "Automated terrain corrected SAR geocoding," in *Proc. IEEE Geosci. Remote Sens. Symp.*, vol. 3, 1999, pp. 1712–1714.

[16] O. Frey, M. Santoro, C. L. Werner, and U. Wegmuller, "DEM-based SAR pixel area estimation for enhanced geocoding refinement and radiometric normalization," *IEEE Geosci. Remote Sens. Lett.*, vol. 10, no. 1, pp. 48–52, Jan. 2013.

[17] G. Fornaro, F. Serafino, and F. Soldovieri, "Three-dimensional focusing with multipass SAR data," *IEEE Trans. Geosci. Remote Sens.*, vol. 41, no. 3, pp. 507–517, 2003.